Evaluating densification of blended elemental (BE) TiPt through pressureless sintering

Z. Gxowa, S. Chikosha and H.K. Chikwanda

Council for Scientific and Industrial Research, South Africa

This work evaluates the densification of blended elemental (BE) Ti-50at.%Pt through pressureless sintering. Titanium hydride dehydride (TiHDH) and platinum powders were blended together in a tubular mixer for 30 minutes. Characterisation of the BE powder was done with the aid of a MICROTRAC Bluewave® particle size and shape analyser and JEOL JSM-6510® scanning electron microscope (SEM). The BE powder was then cold (*i.e.* ambient temperature) compacted to produce green compacts. Green compacts were subjected to conventional pressureless sintering in a horizontal CARBOLITE tube furnace with an argon atmosphere. Sintering was carried out at 1300 and 1400°C for 6, 12 and 24 hours. Density was measured by Archimedes' principle using an OHAUS Explorer® density kit. Micrographs of the sintered samples were taken and the porosity was estimated from binary images using IMAGE J® 1.46r. Challenges were experienced with achieving full (*i.e.* 100%) density with pressureless sintering. This was attributed to the difference in diffusion rates of Ti and Pt, where Ti was assumed to be diffusing faster than Pt; thus creating vacancies which ultimately led to porosity. This phenomenon of pore formation due to differing diffusion rates during sintering is known as the Kirkendall effect. It was concluded that to achieve good densification in powder metallurgically produced TiPt, mechanically alloyed powders which are already homogenised should be used in order to minimise the Kirkendall effect. If BE powders are used, pressure-assisted sintering, *e.g.* spark plasma sintering (SPS) should be used to improve densification.

INTRODUCTION

Shape memory alloys (SMAs) are materials that have the ability to revert to their original shape if, after deformation, they are heated at the correct transition temperature (Sun *et al*., 2012). This shape recovery occurs as a result of a reversible martensitic transformation which takes place at a certain transition temperature (unique to each SMA) (Araya, 2012). SMAs may find application in various industries such as medical, automotive and aerospace as couplings or actuators (Jani *et al*., 2014). In the automotive industry, SMAs are required to perform at temperatures between 100 and 300°C and application temperatures of up to 1000°C are required in the aerospace industry (Padula *et al*., 2006). NiTi-based alloys are the commercially available SMAs, but their use in the automotive and aerospace industries is limited due to the fact that their maximum application temperature is 100°C (Jani *et al*., 2014). This has led to the demand for high-temperature shape memory alloys (HTSMAs) with application temperatures above 100°C. To expand the application spectrum of SMAs, there is ongoing research to develop HTSMAs that can meet the highest application temperature demand of 1000°C. Titanium-platinum (TiPt) alloys have potential application as HTSMAs due to the presence of a martensitic transformation which occurs at 1050°C (Araya, 2012).

HTSMAs are conventionally produced by melting, which entails high energy costs and challenges with producing a homogeneous alloy (Green *et al*., 1997). The high costs incurred in the melting process are due to high melting temperatures needed to make the alloy (influenced by melting points of metals) as well as remelting which is done to improve homogeneity of the alloy (Green *et al*., 1997). Powder metallurgy (PM) offers a potential solution to these issues as it is considered an alternative to melting due to lower energy costs, minimal machining and reduced oxidation (James, 2015). Examples of powder metallurgical processes include press and sinter (*i.e.* pressureless sintering), metal injection moulding, powder extrusion and direct powder rolling (Johnson, 2000). Press and sinter is considered the oldest, most understood and cheapest powder processing method (Qian *et al*., 2010). In PM, blended elemental (BM) or pre-alloyed (PA) powders may be used; the BE approach has been reported to be more cost-effective (Liu *et al*., 2006). BE powders also have better compressibility than PA powders (Wang *et al*., 2010).

Ivasishin *et al*. (2002) stated that to achieve good mechanical properties (*e.g*. hardness and tensile strength), sintered materials should not only have a homogeneous microstructure and chemical composition but also a relative density of at least 98%. Peng *et al*. (2016) discussed the effect of densification on mechanical properties and made reference to PM-produced parts which had porosity ranging from 5 to 15%. It was found that this porosity lowered mechanical properties such as strength and hardness (Peng *et al*., 2016). According to Peng *et al*. (2016) this low densification reduced the application spectrum of these components in the automotive industry because their mechanical properties were lower than the desired level. Chawla and Deng (2003) observed that when densification was improved by decreasing porosity, mechanical properties such as tensile strength, Young's modulus and fatigue resistance improved. Poor densification leads to poor mechanical properties because pores reduce the load-bearing capacity of materials by reducing the effective load-bearing cross-sectional area, and pores may become crack initiation sites (Chawla and Deng, 2003; Channankaiah and Ranganath, 2012). It is evident that properties such as strength and performance are directly influenced by density (Suresh *et al*., 2015). It can be said that densification determines structural integrity of products (Eck *et al*., 2014). Thus, in developing TiPt HTSMAs using PM attention has to be paid to the amount of densification achieved since it will have a significant influence on structural integrity and ultimately performance.

This work evaluates the densification of blended elemental (BE) Ti-50at.%Pt through pressureless sintering. The results obtained from this work are significant because they will give an indication of how much densification can be achieved through pressureless sintering, which will help assess if the cheapest PM technique of press and sinter (presureless sintering) is suitable for densification and if it can be used as an alternative to melting.

EXPERIMENTAL PROCEDURE

Titanium hydride dehydride (TiHDH -45 µm) with 99.5 purity supplied by Baoji, Lihua Non-Ferrous Metals Co., Ltd and platinum (Pt -250 µm) of 99.99% purity supplied by Anglo American-Platinum powders were blended together in a tubular mixer for 30 minutes to produce blended elemental (BE) TiPt powder. Characterisation of the BE powder was done with the aid of a MICROTRAC Bluewave® particle size and shape analyser and JEOL JSM-6510® scanning electron microscope (SEM). The BE powder was then cold (*i.e.* ambient temperature) compacted using an ENERPAC VLP® 100 t press to produce green compacts (d = 8 mm, h = approx. 2 mm). The size of the green compacts was kept small for economic reasons; Pt powder is expensive (currently about $987.30 per ounce). The compressibility of the TiPt powder was assessed by pressing several 1g samples at 10-100 bar and measuring their densities with the aid of an OHAUS Explorer® density kit. Green compacts were subjected to conventional pressureless sintering in a horizontal CARBOLITE tube furnace with an argon atmosphere. Sintering was carried out at 1300 and 1400°C for 6, 12 and 24 hours. Densities of sintered samples were measured by applying Archimedes' principle using an OHAUS Explorer® density kit. Micrographs of the sintered samples were taken and the porosity was estimated from binary images using IMAGE J® 1.46r. X-ray diffraction (XRD) analysis was done on the green compacts using a

PANalytical X-pert® X-Ray diffractometer (XRD) with Cu Kα radiation (λ=1.5406Å). A Ni filter was used to filter out unwanted X-rays. XRD analysis was done over a 2θ range of 20-120°C and the scan rate was 58.14 seconds per step. The X'Pert-HighScore® analysis software package was used to study the resulting diffraction patterns and phases were identified using reference databases available on the software package.

RESULTS AND DISCUSSION

Characterisation of BE powder

The blended elemental (BE) TiPt powder consisted of spongy, slightly larger Pt and smaller, irregularly shaped Ti powder particles (Figure 1). From Figure 2 it can be observed that the BE powder had a bimodal particle size distribution (PSD) which is shown by two peaks; a smaller (approx. 7.78-74 µm) and larger (approx. 74-296 µm) peak. It was thought that the smaller peak corresponds to Ti (which is a -45 µm powder) and some smaller Pt powder particles while the larger peak corresponds to Pt powder particles (-250 µm powder). Figure 1 strongly supports this notion.

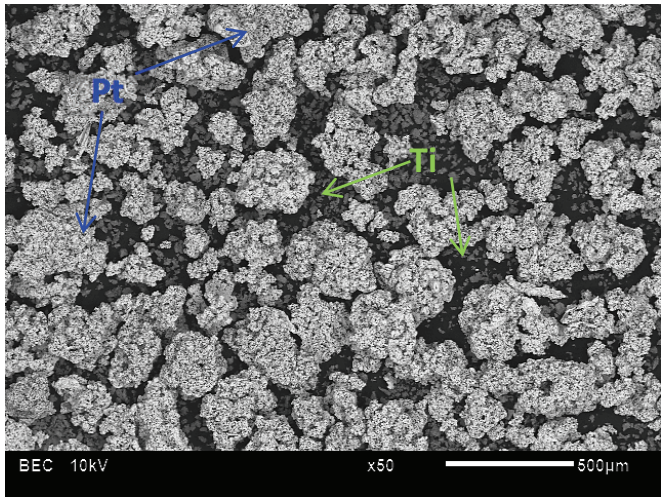

Figure 1. SEM BSE micrograph of blended elemental (BE) TiPt powder.

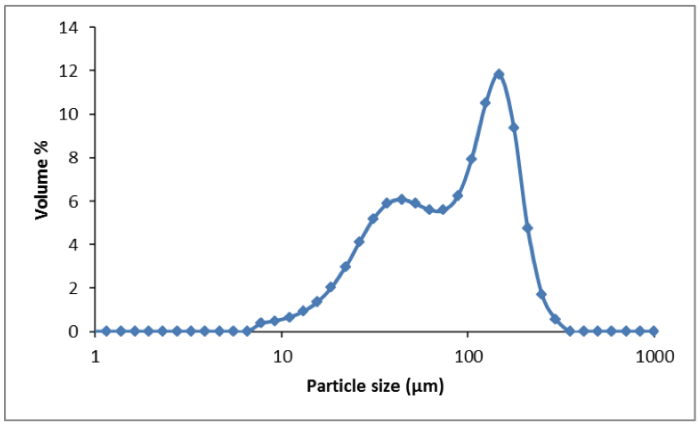

Figure 2. PSD curve of blended elemental (BE) TiPt powder.

Compaction

The ENERPAC press that was used to construct the compressibility curve shown in Figure 3 works in such a way that the pressure applied by the anvil to the powder is set using a gauge meter which is

connected to the press. The maximum allowable gauge meter reading is determined by die diameter so, for the 8mm diameter die used in this work the maximum allowable guage meter reading is 100 bar (equivalent to 2842 MPa). The compressibility curve for the BE TiPt powder shows that a range of pressures were used to press the BE powder (Figure 3). It can be observed that relative density increases with an increase in pressure. Higher pressure may have improved bonding between particles and resulted in better densification (*i.e.* higher relative density). It can be observed that at the highest allowable pressure, a relative density of 97.89% was achieved. The cold compaction process at high pressures resulted in relatively high green densities; however, it may not be ideal on an industrial scale since these high pressures may shorten service life of compaction equipment (Rao *et al*., 1999).

Figure 4 shows that the Ti and Pt particles mechanically bonded as a result of cold compaction and very small pores can be observed for the samples compacted at 2842 MPa. Density measurements of the 2842 MPa compacted samples showed that the green compacts had high relative densities of 97.89%, and the micrograph shown in Figure 4 corroborates the density result. XRD analysis on the green compacts showed that there was no interdiffusion between Ti and Pt to form new phases during cold compaction, since individual Ti and Pt peaks were detected as shown in Figure 5. This result was expected because there was no driving force for interdiffusion during cold compaction. Figure 4 shows that good densification was achieved by compaction at 2842 MPa pressure; however, at this stage the desired homogeneous single phase TiPt alloy and a metallurgical bond between particles had not been formed yet. To form this homogeneous TiPt alloy and metallurgical bonding, diffusion would have to take place and pressureless sintering was used to drive this diffusion process. The atomic diffusion which occurs as a result of sintering improves strength because it converts the mechanical bonds which exists amongst particles in the green compacts into stronger metallurgical bonds (Totten *et al*., 2002).

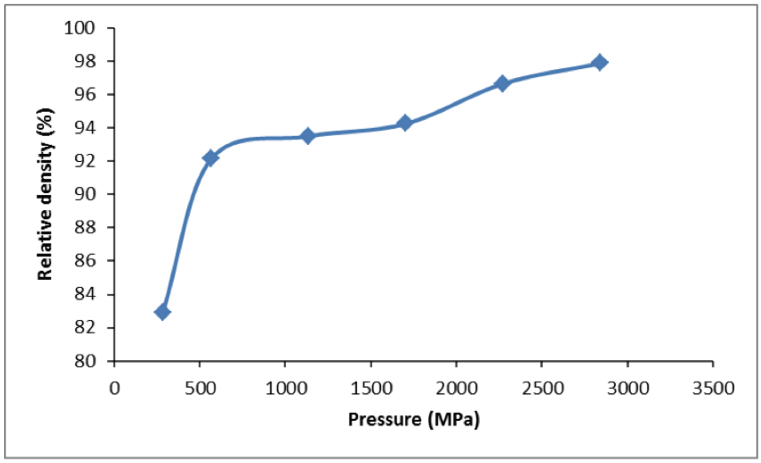

Figure 3. Compressibility curve for blended elemental (BE) TiPt.

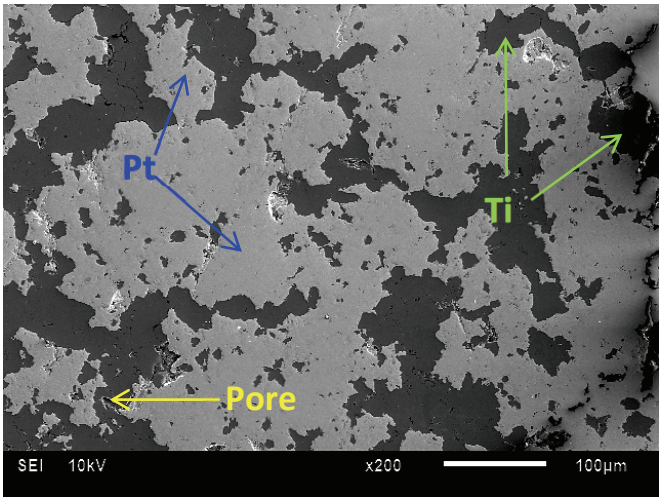

Figure 4. Green compact made from blended elemental (BE) powder pressed at 100 bar.

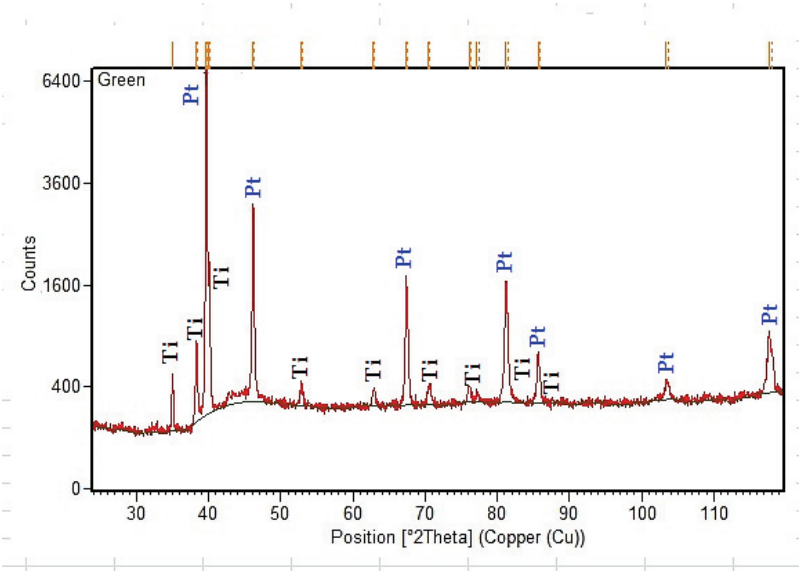

Figure 5. XRD pattern for green compact made from BE powder.

Sintering

The ideal situation would be to form a single-phase TiPt alloy while achieving good densification (*i.e.* at least 98%). Ivasishin *et al.*(2002) stated that to achieve good mechanical properties (*e.g.* hardness and tensile strength), sintered materials should not only have a homogeneous microstructure and chemical composition but a relative density of at least 98% as well. Figure 6 shows that after sintering at 1300°C for 2 hours porosity, which was previously not present, had formed. When Figure 4 (green compact) and Figure 6 (sintered compact) are compared, it can be seen that the pores have formed on the boundaries of Pt grains where Ti was situated prior to sintering. This is corroborated by the backscatter image of the sintered alloy in Figure 6b, which shows that the corresponding porous regions are the previously titanium-rich regions.

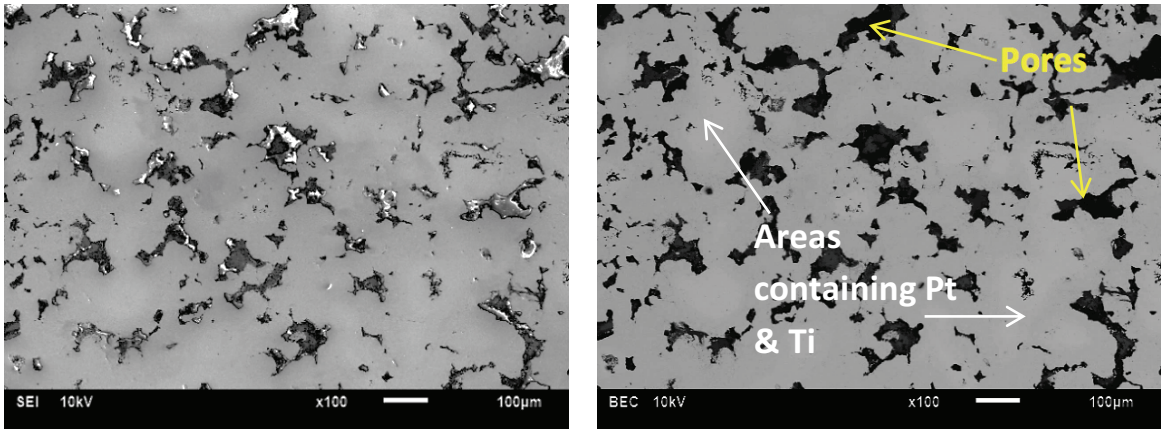

a *b*

Figure 6. SEM (a) SEI and (b) BSE micrographs of BE TiPt sintered at 1300°C for 2 h.

Figure 7 shows that porosity was still present after sintering at 1300°C for 6, 12 and 24 hours. The porosity observed at all these sintering conditions was higher than the starting porosity, which is uncommon behaviour during normal sintering progression. Introduction of sintering temperature and increasing sintering time was expected to result in reduced porosity compared to the starting porosity and hence higher density. This was not the case for this alloy, and further porosity studies were done to quantify the porosity using Image J® 1.46r. The results are shown in Figure 8.

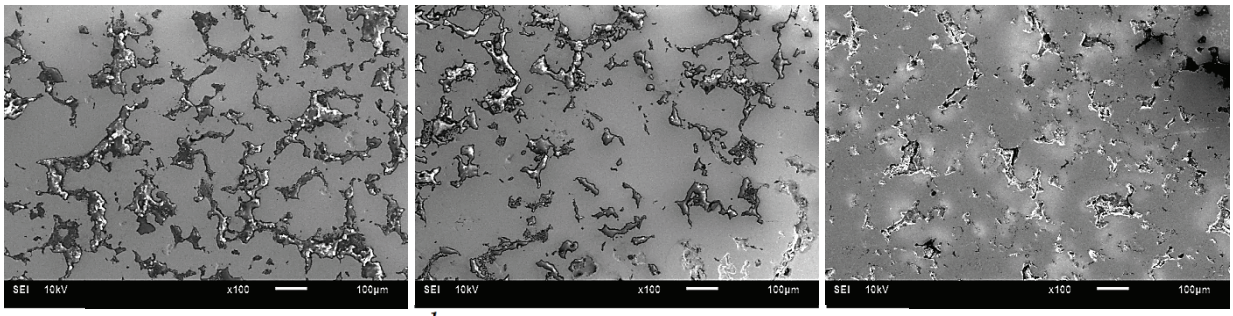

a *b* *c*

Figure 7. SEM SEI micrographs of BE TiPt sintered at 1300°C for (a) 6 h, (b) 12 h and (c) 24 h (scale bar 100 µm).

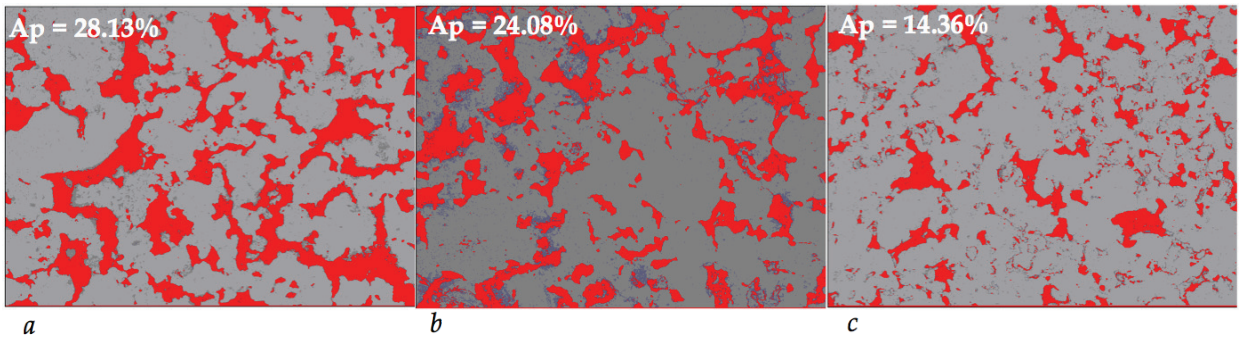

a *b* *c*

Figure 8. Binary images showing area fraction of pores in compacts sintered at 1300°C for (a) 6h, (b) 12 h and (c) 24 h.

To determine the unexpected cause of increasing porosity with sintering, micrographs of sintered samples, at a higher magnification (*i.e.* 500×) and using the backscatter mode were taken. This revealed that the microstructures consisted of various regions which differed in colour and orientation.

Energy dispersive spectroscopy (EDX) analysis showed that these regions differed in composition as well, which indicated that different phases had formed as a result of interdiffusion between Ti and Pt during sintering. Some of the phases that were identified through EDX analysis were: the desired TiPt phase (darker grey), a Ti_3Pt_5 phase with a needle-like structure, as well as a lighter, wavy $TiPt_3$ phase (Figure 9). Figure 9 also shows that the black regions are pores. The formation of pores/voids was thought to be due to a well-known phenomenon called the Kirkendall effect, which has been observed in many binary systems such as Ag-Au, Cu-Sb, Mo-Ti and Au-Ni (van Dal, 2001).

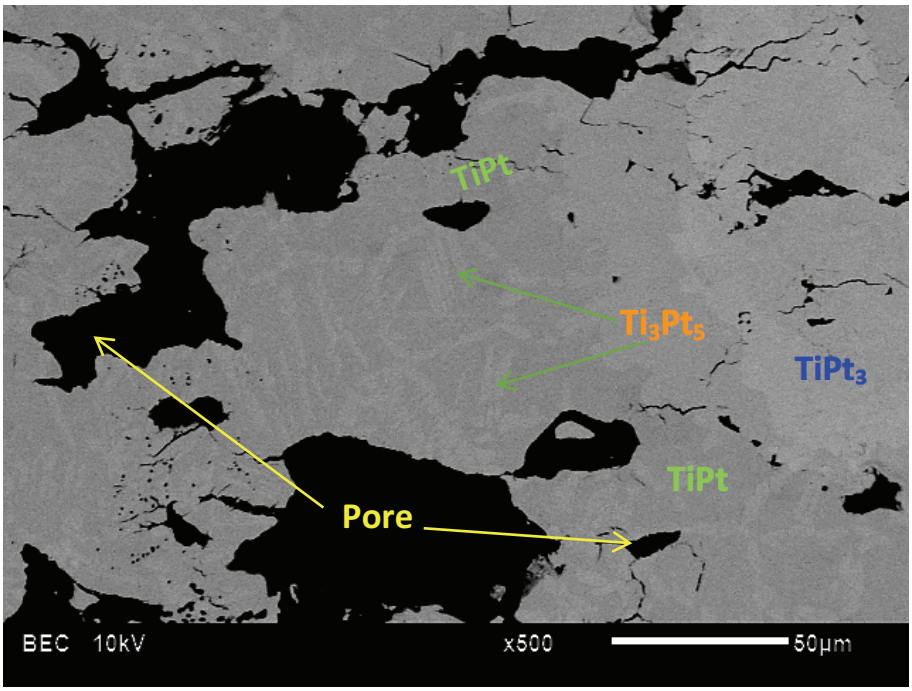

Figure 9. SEM BEI micrograph showing some of the phases which were identified through EDX analysis.

The Kirkendall effect often manifests during sintering in binary systems where the two materials diffuse at different rates. It occurs by a vacancy diffusion mechanism (Cao, 2017). In any binary system where the two materials in the system diffuse at different rates, there will be a net flux (quantified in terms of number or mass) of atoms and a net flux of vacancies moving in opposite directions. This is due to the fact that atoms move in the material by exchanging places with vacancies. Voids are formed in areas where the material with the higher diffusion rate was situated, because vacancies move in a direction opposite to the atoms. These vacancies tend to aggregate and form voids, which are referred to as Kirkendall voids. The fact that voids formed in areas that were previously Ti-rich (Figure 4) led to the assumption that in this TiPt alloy, Ti was diffusing at higher rate than Pt.

Kirkendall voids reduce densification and thus have an adverse effect on mechanical properties (Dutta and Bose, 2012). The formation of Kirkendall voids is thus undesirable. At 1300°C, more voids formed with all sintering conditions compared to starting ones; however, the area fraction of pores (Ap) decreased with an increase in holding time (Figure 8), where the longest holding time (*i.e.* 24 hours) resulted in the lowest fraction of pores. This result suggests that a longer holding time allowed pores to decrease in size and for some to close, which is typical sintering behaviour. A similar trend was observed at 1400°C where the Ap decreased even further (Figures 10 and 11). Figure 11c shows that at 1400°C a holding time of 24 hours decreased the Ap to approximately 3.45%. It can also be observed that the size and shape of the pores also changed. Pores became smaller and more rounded with an increase in temperature and time. This result is interesting because many authors have reported the formation of Kirkendall voids in binary systems with materials with dissimilar diffusion rates, but no literature was found on the reduction in size and quantity of Kirkendall voids as a result of sintering temperature and time.

The effects of temperature and time on porosity were further investigated by sintering green compacts at 1500°C for 24 hours, and only a few pores were observed (Figure 12a). Figures 12a and 12b show that porosity was reduced compared to 1300°C (Figures 6 and 7) and 1400°C (Figure 10). However, the area fraction of pores could not be estimated because of the new darker grey phase (shown by green arrows in Figure 12b) that formed. The area fraction of the pores is estimated from binary images, therefore since the method relies on thresholding the pores, as well as the darker grey phase, would appear dark and yield the wrong result since the darker phase would be mistaken for pores (Roy *et al.*, 2006). EDX analysis showed that the darker phase contains 52.46 at.% titanium, 47.44 at.% oxygen and 0.10 at.% platinum. According to the TiPt phase diagram, 0.10% Pt at 1500°C corresponds to β-Ti. The EDX analysis also showed that sintering at 1500°C for 24 hours resulted in a fairly homogeneous composition since it showed that the dominant, grey areas in Figure 12 are TiPt, which is the desired phase.

To improve understanding of effect of temperature and time on Kirkendall voids, in future work microfocus X-ray computer tomography (CT) will be used to further quantify porosity. CT scanning may be useful because it can provide three-dimensional (3D) images of the sintered samples from which pore size, shape and quantity can be characterised and quantified (du Plessis *et al.*, 2014).

Density measurements showed that relative densities achieved after sintering ranged from 84.35–96%. The highest relative density of 96% was achieved when sintering was carried out at 1500°C for 24 hours. It can be deduced that full densification (*i.e.* 100%) was not achieved through pressureless sintering. The recommended minimum relative density after sintering is at least 98% (Ivasishin *et al.*, 2002), which was not achieved through pressureless sintering. It was concluded that for this alloy, the use of press and sinter of blended elemental powders would not be a viable option for making the TiPt alloy. It is thought that to achieve good densification in powder metallurgically produced TiPt, alloyed powders that are already homogenised should be used in order to minimise the Kirkendall effect. If BE powders are used, pressure-assisted sintering, *e.g.* spark plasma sintering (SPS) should be used to improve densification. SPS has also been reported to have the advantage of producing very dense compacts using sintering times that are much shorter than conventional sintering (Tokita, 2011).

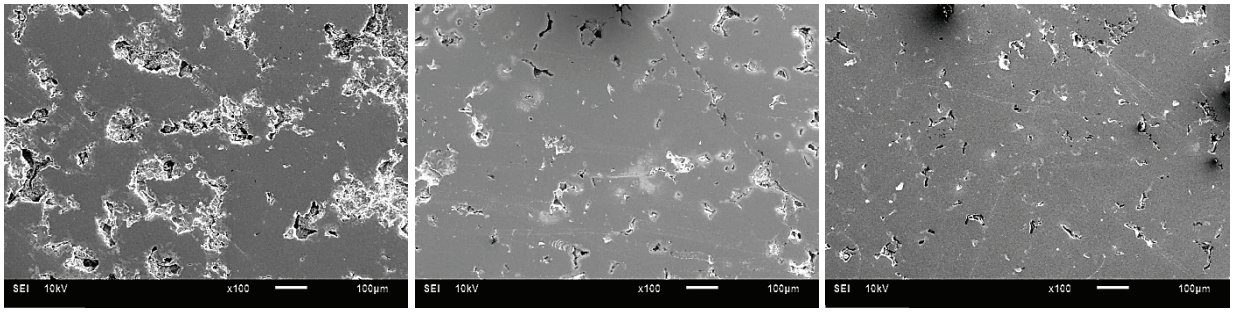

Figure 10. SEM SEI micrographs of BE TiPt sintered at 1400°C for (a) 6 h, (b) 12 h and (c) 24 h (scale bar 100 µm).

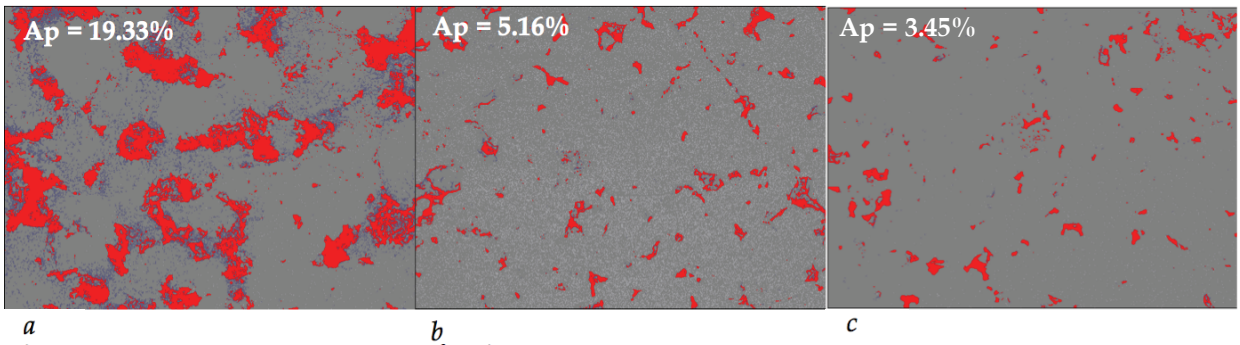

Figure 11. Binary images showing area fraction of pores in compacts sintered at 1300°C for (a) 6 h, (b) 12 h and (c) 24 h.

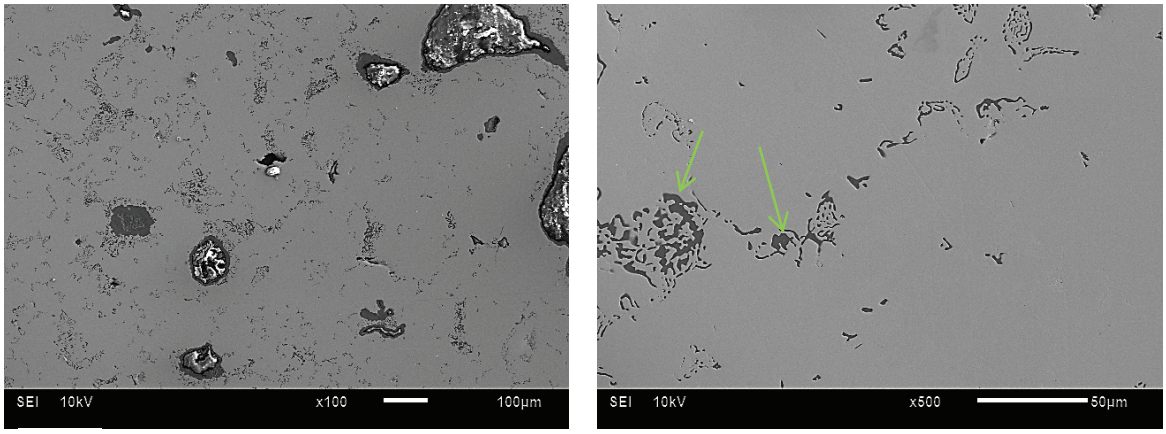

a *b*

Figure 12. SEM SEI micrographs of BE TiPt sintered at 1500°C. (a) Scale bar 100 µm, (b) scale bar 50 µm.

CONCLUSION

The densification of blended elemental (BE) Ti-50at.%Pt through pressureless sintering was investigated, and the following conclusions were drawn.

1. High (*i.e.* at least 98%) or full (100%) densities were not achieved through pressureless sintering of Ti-50at.%Pt blended elemental alloy powders, which suggested that pressureless sintering is not a suitable densification technique for Ti-50at. %Pt alloys.
2. Kirkendall voids formed as a result of pressureless sintering; however, at both 1300 and 1400°C an increase in sintering time from 6 to 24 hours seemed to reduce the quantity and size of the Kirkendall voids.
3. Sintering at 1500°C for 24 hours resulted in a fairly homogeneous microstructure.

ACKNOWLEDGEMENTS

The platinum sponge used in this work was supplied by Anglo American Platinum through funding for research proposal number 4/2010.

REFERENCES

Araya, K.E.T. (2012). Phase transformations and equilibria of titanium platinum alloys in the composition range 30-50 atomic percent platinum . PhD thesis, Colorado School of Mines.

Cao, G. (2017). Atomic level understanding of the nanoscale Kirkendall effect. *Science Bulletin*, *62* (12), 818–819. http://doi.org/10.1016/j.scib.2017.05.006

Channankaiah, F.Z. and Ranganath, G. (2012). Experimental approach on densification and mechanical properties of sintered powder metallurgy AISI 4140 steel preforms. *ARPN Journal of Engineering and Applied Sciences*, 7 (3), 298–303.

Chawla, N. and Deng, X. (2003). Effect of density on the microstructure and mechanical behavior of powder metallurgy Fe-Mo-Ni steels. *Mechanical Behaviour of Materials,* 6, 7-257.

Du Plessis, A., Seifert, T., Booysen, G. and Els, J. (2014). Microfocus X-ray computed tomography (CT) analysis of laser sintered parts. *South African Journal of Industrial Engineering*, 11 (2), 109–117. http://doi.org/10.13748/j.cnki.issn1007-7693.2014.04.012

Dutta, G. and Bose, D. (2012). Effect of Sintering temperature on density, porosity and hardness of a powder metallurgy component. *International Journal of Emerging Technology and Advanced Engineering*, *2* (8), 121–123.

Eck, S., Ecker, W., Wlanis, T., Gänser, H.P. and Ebner, R. (2014). Through process modelling of surface densified PM gears. *BHM Berg- Und Hüttenmännische Monatshefte*, 159 (9), 371–374. http://doi.org/10.1007/s00501-014-0283-8

Green, M., Grant, D. M. and Kelly, N. R. (1997). Powder metallurgical processing of Ni-Ti shape memory alloy. *Powder Metallurgy*, 40 (1), 43–47. http://doi.org/10.1179/pom.1997.40.1.43

Ivasishin, O.M., Savvakin, D G., Froes, F.H. and Bondareva, K.A. (2002). Synthesis of alloy Ti-6Al-4V with low residual porosity by a powder metallurgy method. *Powder Metallurgy and Metal Ceramics*, 41 (7-8). 382–390. http://doi.org/10.1023/A:1021117126537

James, W. B. (2015). Powder metallurgy methods and applications. *ASM Handbook*, vol. *7.* Powder Metallurgy. ASM INternational, Materials Park, OH. p. 922.

Jani, J. M., Leary, M., Subic, A. and Gibson, M.A. (2014). A review of shape memory alloy research, applications and opportunities. *Materials and Design*, 56, 1078–1113. http://doi.org/10.1016/j.matdes.2013.11.084

Johnson, P.K. (2000). Powder metallurgy. *Kirk-Othmer Encyclopedia of Chemical Technology*. Wiley, Hoboken, NJ. http://doi.org/10.1002/0471238961.1615230410150814.a01

Liu, Y., Chen, L.F., Tang, H.P., Liu, C.T., Liu, B. and Huang, B.Y. (2006). Design of powder metallurgy titanium alloys and composites. *Materials Science and Engineering A*, 418 (1-2), 25–35. http://doi.org/10.1016/j.msea.2005.10.057

Padula, S., Bigelow, G., Noebe, R., Gaydosh, D. and Garg, A. (2006). Challenges and progress in the development of high-temperature shape memory alloys based on NiTiX compositions for high-force actuator applications. *Proceedings of the International Conference on Shape Memory and Superelastic Technologies.* http://doi.org/10.1361/cp2006smst787

Peng, J., Zhao, Y., Chen, D., Li, K., Lu, W. and Yan, B. (2016). Effect of surface densification on the microstructure and mechanical properties of powder metallurgical gears by using a surface rolling process. *Materials*, 9 (10). http://doi.org/10.3390/ma9100846

Qian, M., Schaffer, G. and Bettles, C. (2010). Sintering of titanium and its alloys. *Sintering of Advanced materials:Fundamentals and Processes*. Fang, Z.Z. (ed.), Woodhead Publishing, Philadelphia:. p. 324.

Rao, B.K., Khadar, M.S.A and Srinivasan, K. (1999). High temperature compression testing and determination of warm working temperature for commercial purity aluminium. *Bulletin of Materials Science*, 22 (1), 17–20. http://doi.org/10.1007/BF02745670

Roy, T.K., Subramanian, C. and Suri, A. K. (2006). Pressureless sintering of boron carbide. *Ceramics International*, 32 (3), 227–233. http://doi.org/10.1016/j.ceramint.2005.02.008

Sun, L., Huang, W.M., Ding, Z., Zhao, Y., Wang, C.C., Purnawali, H. and Tang, C. (2012). Stimulus-responsive shape memory materials: A review. *Materials and Design*, 33 (1), 577–640. http://doi.org/10.1016/j.matdes.2011.04.065

Suresh, K. ., Mahendran, S., Krupashankara, M.and Avinash, L. (2015). Influence of powder composition morphology on green density for powder metallurgy processes. *International Journal of Innovative Research in Science, Engineering and Technology*,4 1, 18629–18634. http://doi.org/10.15680/IJIRSET.2015.0401037

Tokita, M. (2011). Mechanism of spark plasma sintering.*Ceramics*, 605–608. http://doi.org/10.1063/1.3622584

Totten, G., Howes, M. and Inoue, T. (eds.). (2002). Powder metallurgy parts manufacturing. *Handbook of Residual STress and Deformation of Steel*. ASM International, Ohio . p. 398.

Van Dal, M.J.H. (2001). Microstructural stability of the Kirkendall plane. Master's thesis, Technische Universiteit Eindhoven.

Wang, H.T., Lefler, M., Zak Fang, Z., Lei, T., Fang, S.M., Zhang, J.M. and Zhao, Q. (2010). Titanium and titanium alloy via sintering of TiH_2. *Key Engineering Materials*, 436, 157–163. http://doi.org/10.4028/www.scientific.net/KEM.436.157

Zizo Gxowa

Candidate Researcher
Council for Scientific and Industrial Research (CSIR).

Zizo Gxowa is a Candidate Researcher at the Council for Scientific and Industrial Research (CSIR). She obtained a BSc Eng. (Metallurgy and Materials Engineering) degree from the University of the Witwatersrand in 2014. She is currently undertaking her MSc Eng. (Metallurgy and Materials) degree at the University of the Witwatersrand, under the auspices of the DST-NRF Centre of Excellence in Strong Materials.